Available online at www.sciencedirect.com
SCIENCE DIRECT®
Chemical Physics Letters 410 (2005) 275–281
CHEMICAL PHYSICS LETTERS
www.elsevier.com/locate/cplett

Density functional theory study of adsorption of OOH on Pt-based bimetallic clusters alloyed with Cr, Co, and Ni

J.M. Seminario *[a,b], L.A. Agapito [a,b], L. Yan [a], P.B. Balbuena [a,*]

[a] Department of Chemical Engineering, Texas A&M University, College Station, TX 77843, United States
[b] Department of Electrical and Computer Engineering, Texas A&M University, College Station, TX 77843, United States

Received 20 April 2005; in final form 5 May 2005
Available online 16 June 2005

Abstract

The adsorption of OOH, the main product of the first step in the O_2 reduction on Pt(1 1 1) surfaces, is studied on Pt-based bimetallic three-atom clusters. Cr, Co, and Ni are better adsorption sites for OOH than Pt, but the strong adsorption might not favor the dissociation of OOH. However, the presence of Cr, Co, or Ni in the vicinity of a Pt atom increases its electron density, enhancing the Pt ability to transfer electrons to oxygenated species. Thus, Cr, Co, or Ni in the subsurface, rather than on the exposed surface, may contribute favorably to catalyze the O_2 reduction.

1. Introduction

Searching for alternative oxygen electroreduction (OER) catalysts is an important topic in relation to fuel cell development [1], given the high cost of platinum and the slow kinetics of the OER reaction [2–4]. Alloys of Pt with other less expensive metals can decrease the fuel cell operational costs. Experimental work has indicated that the catalytic activity of Pt-based bimetallic nanoclusters alloyed with Cr, Co, and Ni, towards the OER in acidic medium of polymer exchange membrane fuel cells (PEMFC) is at least as good as that of pure Pt, and in some cases, the bimetallic catalysts yield slightly better oxygen reduction currents than pure Pt [3,5–7]. But the extent of the improvement is not clear, and one of the reasons may be the different constitution of the alloy as determined by the nanocatalyst fabrication procedure.

Several aspects about the various steps of the four-electron OER in acid medium are still in debate, and possible mechanisms have been proposed [8–11]. The overall mechanism could be described as a sequence of steps. Firstly, O_2 diffuses to the Pt surface followed by molecular adsorption on the catalytic electrode, which may include physisorption and chemisorption processes [12,13]. Protonation may precede or follow the adsorption, depending on the degree of proton solvation, and on the proximity of the O_2 molecule to the surface [14–17]. However, in either case, the resultant product is the adsorbed OOH species. Thus, the alternative processes

$$O_2 + e^- \xrightarrow{\text{catalyst}} (M - O_2^-)_{\text{adsorbed}}$$

$$(M - O_2^-)_{\text{adsorbed}} + H^+ \xrightarrow{\text{catalyst}} (M - OOH)_{\text{adsorbed}}$$

or a coupled electron transfer and proton transfer

$$O_2 + e^- + H^+ \xrightarrow{\text{catalyst}} (M - OOH)_{\text{adsorbed}}$$

are considered the rate-determining step, resulting in the formation of end-on adsorption of OOH [15–17]. The

* Corresponding author. Fax: +979 845 6446.
E-mail addresses: seminario@tamu.edu (J.M. Seminario), balbuena@tamu.edu (P.B. Balbuena).

0009-2614/$ - see front matter © 2005 Elsevier B.V. All rights reserved.
doi:10.1016/j.cplett.2005.05.077

adsorbed end-on OOH may rearrange yielding a bridge adsorption with both O atoms adsorbed; in both cases (end-on or bridge adsorption) adsorption should be followed by dissociation of the O–O bond and adsorption of OH and O [8,15,16,18,19].

The OER 2nd electron and proton transfer may follow two alternative processes. If a second electron is transferred to the end-on OOH prior to its rearrangement, both the O–metal adsorption bond and the O–O bond are weakened. The following proton transfer may lead to the formation of water and an adsorbed O or hydrogen peroxide depending on which O the proton attacks [15,16]. H_2O_2 is unstable and eventually decomposes into adsorbed O and H_2O. Results of adsorption of hydrogen peroxide on these bimetallic clusters are reported separately. However, the formation of hydrogen peroxide increases the over-potential on the cathode, decreasing the effectiveness of fuel utilization. The adsorption of hydrogen peroxide also reduces the effectiveness of the catalysts, decreasing the current density of the fuel cell. The successive (3rd and 4th) electron and proton steps involve electron transfer and protonation to the O and OH adsorbed species, leading to water formation.

Our recent work demonstrated that clusters containing Pt–X and Pt–X–X (with X = Co or Cr) are best active sites to promote O–O dissociation [4]. We have also analyzed the adsorption of OH and water on the clusters and concluded that the alloyed clusters are stronger adsorbents for both species; therefore they could accumulate on the surface altering or even interrupting the OER process.

In this Letter, the adsorption of O–O–H on various Pt–X–X, and Pt–Pt–X (with X = Co, Cr, and Ni) clusters is studied by first principles density functional theory (DFT) calculations. The most stable structures are identified and their binding energies are reported. The stabilities of the O–O and O–metal bonds are evaluated by analyses of second derivative calculations of the energy. The nature of the attractive sites is also investigated by Mulliken charge distribution analysis.

2. Computational methods

DFT is used to determine optimized structures, binding energies, Mulliken charge distribution, and vibrational frequencies for several metallic clusters and their complexes with OOH. Two types of starting configurations are used to evaluate adsorption of OOH on the clusters, one with the OOH ligand initially on the top site of a metallic atom and another where the OOH ligand is initially located on the hollow site. In order to obtain the lowest energy optimized structure, at least five lowest spin multiplicities are investigated for every system. The structural optimization is followed by a second derivative calculation of the total energy, and all systems are checked so no imaginary vibrational frequencies are present in the optimized geometries. The DFT calculations are run at the B3PW91 level of theory as implemented in the GAUSSIAN 03 program [20]. The B3PW91 level of theory uses the Kohn–Sham (KS) Hamiltonian [21,22] with the Becke-3 hybrid exchange functional [23] and the generalized-gradient approximation (GGA) Perdew–Wang 91 correlation functional [24,25]. DFT methods using hybrid exchange functional and GGA correlation functionals are among the most powerful to deal with metal-small molecule systems [26,27]. The LANL2DZ basis sets as well as effective core potentials [28–31] are used for all metallic elements, and the cc-PVDZ basis sets for O and H [32–34].

3. Results and discussion

3.1. Cohesive energy of mono and bimetallic clusters

The cluster cohesive energy (CE) is calculated as the difference between the energy of the cluster and the sum of the energies for each component atom, calculated with the same functional and basis set. CEs for Pt–Pt–Pt, Pt–Pt–X, and Pt–X–X (with X = Co, Cr, and Ni) clusters of various multiplicities are summarized in Fig. 1. All the optimizations are conducted from an initial geometry without symmetry restrictions; a second derivative calculation proved that the optimized geometries are local minima. The CE for Pt_3 is −5.54 eV, and slight changes are found when a Co, Cr, or Ni atom substitutes one of the Pt atoms; only in the case of $CoPt_2$ the cohesive energy of the cluster is stronger (−5.63 eV)

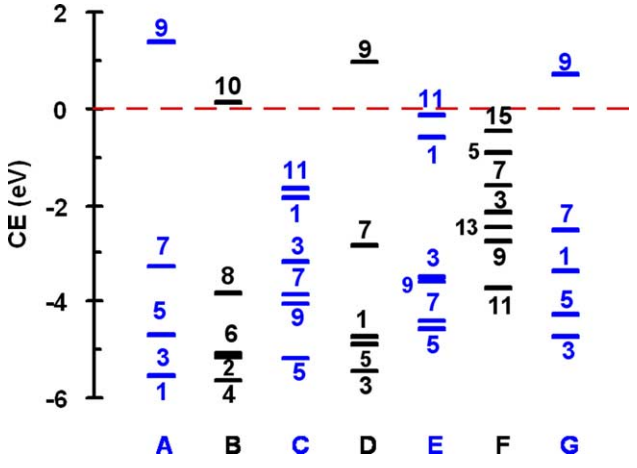

Fig. 1. Cohesive energy (horizontal bars) for Pt_3 (A), $CoPt_2$ (B), $CrPt_2$ (C), $NiPt_2$ (D), Co_2Pt (E), Cr_2Pt (F), and Ni_2Pt (G) in their ground and excited states, obtained from DFT calculations (B3PW91/LANL2DZ); multiplicities are indicated next to the bars. In the first column (A), cohesive energies corresponding to multiplicities 1 and 3 are very close (−5.544 eV for $m = 1$ and −5.539 eV for $m = 3$).

than that of Pt_3. However, the CE decreases in magnitude to −4.35 eV on average when two of the Pt atoms are substituted by a pair of Co, Cr, or Ni atoms.

The Mulliken charge distribution (Fig. 2) indicates that the foreign Co, Cr, and Ni atoms in the Pt-based bimetallic alloy cluster behave as electron donors to the Pt atom; thus Pt becomes negatively charged and would be more attractive to the electrophilic O_2. Cr is the best electron donor, followed by Ni, and then Co. The calculations also indicate that these clusters exhibit large multiplicities in their ground state except for Pt_3.

3.2. OOH binding to Pt-based bimetallic clusters

The binding energy (BE) defined from the reaction: OOH + metallic cluster → complex, is calculated as the energy difference between products and reactants, with the metallic cluster corresponding to its most stable structure (Fig. 1), and a OOH energy of −150.843519 Ha using the B3PW91 functional and cc-pVDZ basis set. The total energies for the reactants are listed in Table 1.

When an OOH group binds to a three-atom metallic cluster, there are four possible geometrical binding configurations: to a single metallic atom (atop-site), to two metallic atoms making a bridge (bridge-site), to three metallic atoms (hollow-site), and two O atoms binding to two metallic atoms making a four member ring (ring-site). Our calculations show that the hollow site configuration is not a local minimum or at most it could be a shallow minimum since no stable hollow site adsorption configurations are found. The optimized configurations are summarized in Fig. 3 and Table 2.

For Pt_3–OOH, two local minima are found (Figs. 3A and B); the atop-site has much lower energy than the bridge-site configuration. Starting from a hollow-site, the optimization may stop at the bridge-site if the GDIIS optimization algorithm [35] is used; however, starting from an atop-site the bridge-site configuration is never reached.

For the $NiPt_2$–O_2H clusters, three local minima are found (Figs. 3C–E). The atop-Ni-site (E) is the most stable configuration, whereas the atop-Pt (D) and Pt–Ni bridge-sites (C) have slightly lower binding energy. If an additional Pt atom is substituted by Ni, a four-member ring-Ni_2O_2-site is found (Fig. 3F), but adsorptions at the bridge-Ni–Ni and another on an atop-Pt-site are also found (Figs. 3G and H). The four-member ring (F) and Ni–Ni bridge-site configurations (G) are much more stable than the atop-Pt-site configuration (H).

The binding between Co and OOH (Fig. 3I–M) is much stronger than that between Pt and OOH. Therefore, an OOH initially on hollow-site is attracted by Co atoms, and will end up strongly bonded to an atop-Co-site (M) or at a bridge-Co–Co-site (L). Also, an OOH starting from an atop-Pt-site can end up either at an atop-Pt-site such as in $CoPt_2$–O_2H (Fig. 3J) or at a ring-$CoPtO_2$-site such as in Co_2Pt–O_2H (Fig. 3K).

Cr has the strongest binding ability towards OOH in the group of metals studied (Figs. 3N–R). The OOH binding energy to an atop-Cr-site is −2.40 eV in $CrPt_2$–O_2H; however, the binding energy to an atop-Pt-site is almost the same as in pure Pt_3. In the Cr_2Pt–O_2H clusters, the Cr atom attracts an atop-Pt-site OOH to a ring-$CrPtO_2$-site, and when initially located on the hollow site, OOH can be dissociated without barrier (R). Analyses of Fig. 3 also indicate that all bimetallic ensembles when complexed with OOH yield elongated O–O distances with respect to that found in Pt_3OOH (1.437 Å in structure B). The O–O bond length values associated with the strongest binding energies (Table 2) in the XPt_2 and X_2Pt complexes range between 1.453 (E) and 1.477 Å (F). The most favorable case, producing the longest elongation of the O–O bond length (1.482 Å) and a weak binding energy (−1.65 eV), is the adsorption on the bridge Pt–Co site of Co_2Pt (Fig. 3K). However, as remarked above, an even better

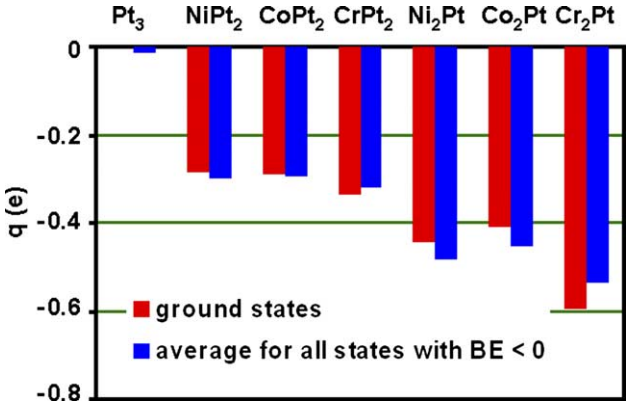

Fig. 2. Mulliken charge on the Pt atom in bimetallic clusters XPt_2 and X_2Pt; the excited states have slightly different charge distribution than the ground states.

Table 1
Total energies for reactants Pt_3 + OOH, Pt_2X + OOH, and PtX_2 + OOH, the multiplicity *m* corresponds to the isolated metallic clusters

Reactants	*m* (cluster)	Energy (ha)
Pt_3 + OOH	1	−508.40278
$CoPt_2$ + OOH	4	−534.33549
$CrPt_2$ + OOH	5	−475.57795
$NiPt_2$ + OOH	3	−558.56199
Co_2Pt + OOH	5	−560.22601
Cr_2Pt + OOH	11	−442.71247
Ni_2Pt + OOH	3	−608.69734

ensemble for OOH dissociation was found in the Cr_2Pt cluster (Fig. 3R) which dissociates OOH without barrier.

The OOH binding energies to a Pt-based bimetallic cluster are summarized in Fig. 4, which displays the relative BEs of the ground states as well as those of the ex-

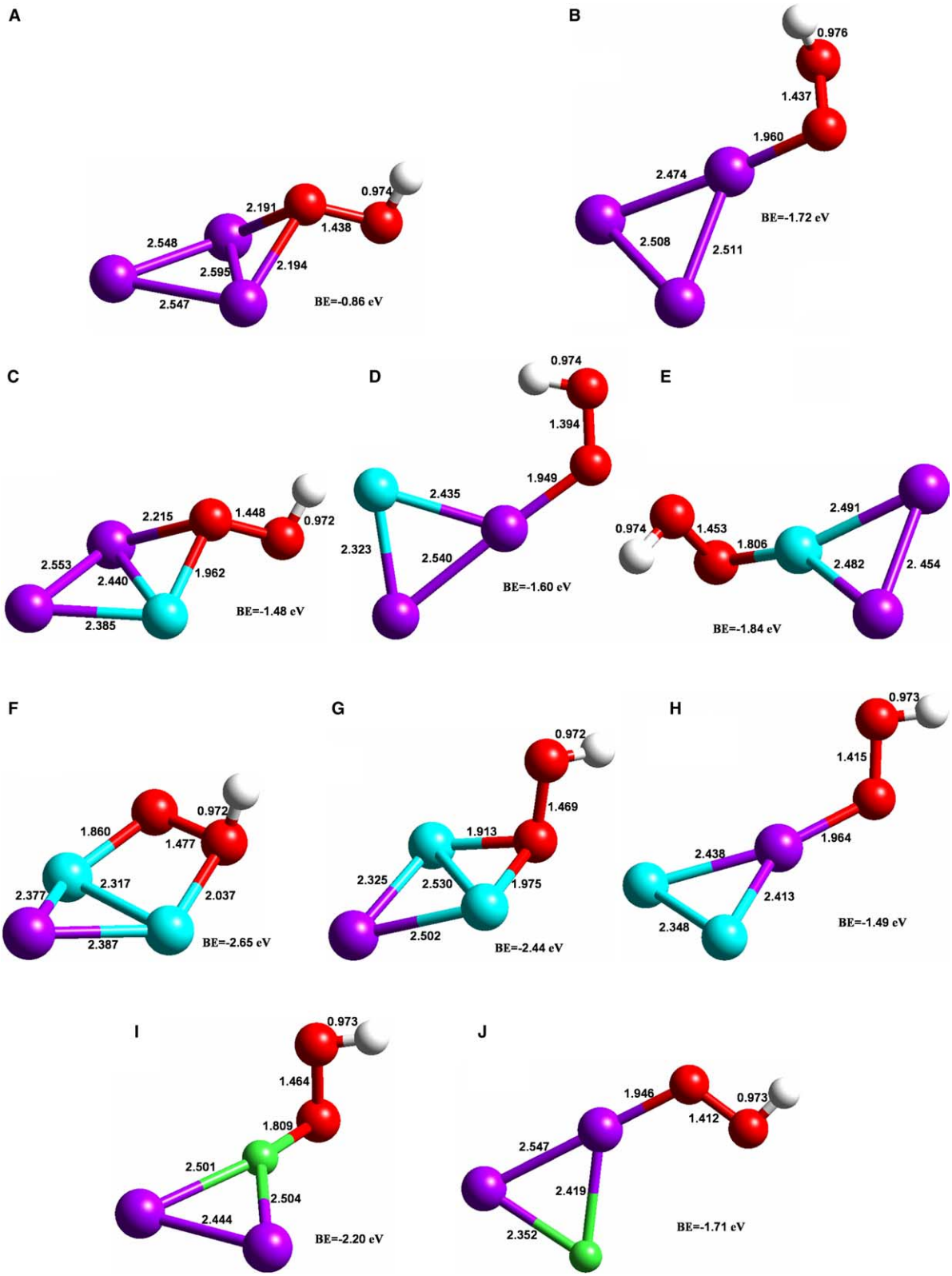

Fig. 3. Geometrical configurations of local minima for the Pt-based bimetallic clusters complexed with an OOH ligand. Pt: purple, Ni: blue, Co: green, Cr: brown, O: red, H: white. (For interpretation of the references to color in this figure legend, the reader is referred to the web version of this article.)

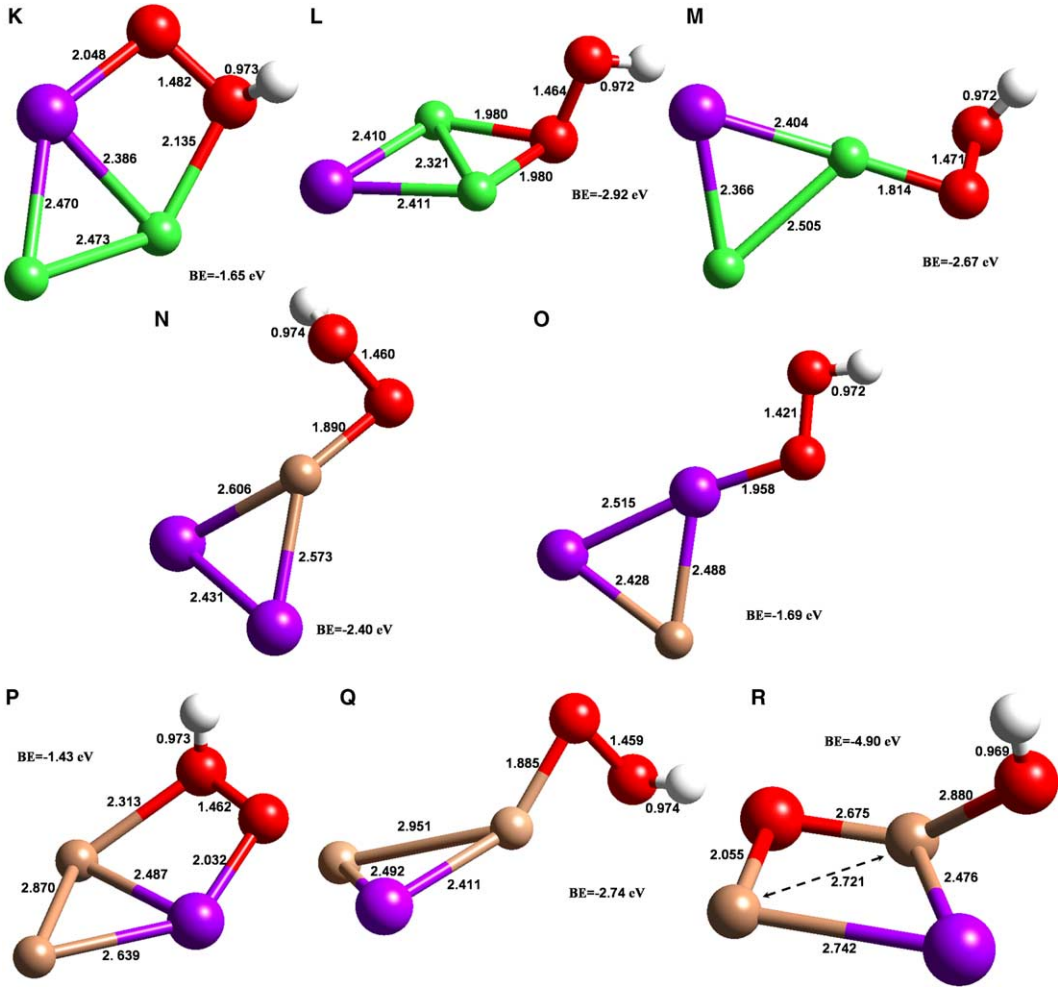

Fig. 3 (*continued*)

Table 2
Starting and adsorption sites for adsorption of OOH on bimetallic clusters, binding energy (BE), and O–O bond distance

Stoichiometry	*m*	Starting site	Adsorption site	BE (eV)	Structure	O–O (Å)
Pt_3–OOH	2	Atop-Pt	Atop-Pt	−1.72	B	1.437
Pt_3–OOH	4	Hollow-site	Bridge-PtPt	−0.86	A	1.438
$NiPt_2$–OOH	2	Atop-Ni	Atop-Ni	−1.84	E	1.453
$NiPt_2$–OOH	4	Atop-Pt	Atop-Pt	−1.60	D	1.394
$NiPt_2$–OOH	4	Hollow-site	Bridge-NiPt	−1.48	C	1.448
Ni_2Pt–OOH	4	Atop-Ni	Ring-NiNiOO	−2.65	F	1.477
Ni_2Pt–OOH	4	Atop-Pt	Atop-Pt	−1.49	H	1.415
Ni_2Pt–OOH	4	Hollow-site	Bridge-NiNi	−2.44	G	1.469
$CoPt_2$–OOH	5	Atop-Co	Atop-Co	−2.20	I1	1.464
$CoPt_2$–OOH	5	Atop-Pt	Atop-Pt	−1.70	J	1.412
$CoPt_2$–OOH	3	Hollow-site	Atop-Co	−2.20	I2	1.464
Co_2Pt–OOH	6	Atop-Co	Atop-Co	−2.67	M	1.471
Co_2Pt–OOH	6	Atop-Pt	Ring-CoPtOO	−1.65	K	1.482
Co_2Pt–OOH	6	Hollow-site	Bridge-CoCo	−2.92	L	1.464
$CrPt_2$–OOH	6	Atop-Cr	Atop-Cr	−2.40	N1	1.460
$CrPt_2$–OOH	6	Atop-Pt	Atop-Pt	−1.69	O	1.421
$CrPt_2$–OOH	4	Hollow-site	Atop-Cr	−2.40	N2	1.460
Cr_2Pt–OOH	2	Atop-Cr	Atop-Cr	−2.74	Q	1.459
Cr_2Pt–OOH	2	Atop-Pt	Ring-CrPtOO	−1.43	P	1.462
Cr_2Pt–OOH	4	Hollow-site	Diss	−4.90	R	∞

The structures correspond to those in Fig. 3.

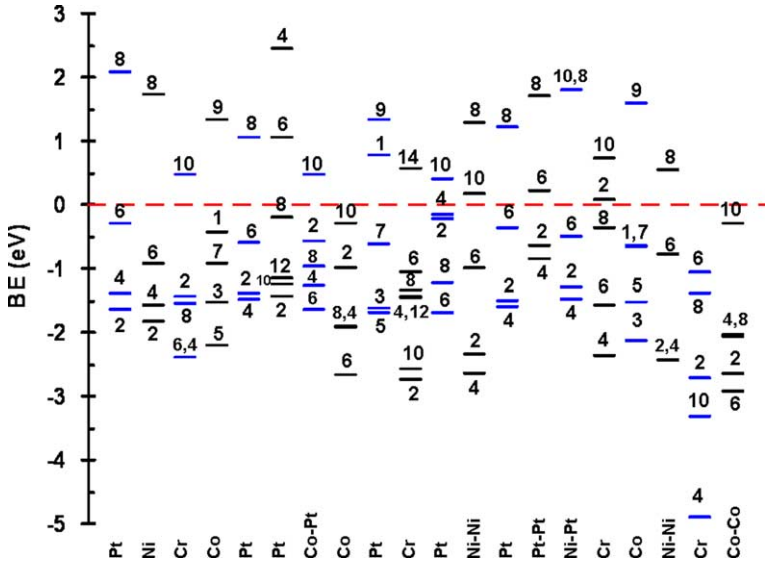

Fig. 4. OOH binding energies to Pt-based bimetallic alloy clusters corresponding to the multiplicities indicated by the numbers. The columns from left to right correspond to the final geometries B, E, N1, I1, H, P, K, M, J, Q, O, F, D, A, C, N2, I2, G, R and L shown in Fig. 3 and Table 2. The labels shown at the bottom indicate the adsorption site of the ground state. In the first thirteen columns the systems had atop-site initial geometries; hollow-site initial configurations were used for the others.

cited states in each case. The graph clearly illustrates the enhancement of the binding energies produced by substitution of one or more atoms of Pt by Ni, Cr, and Co. On the other hand, the binding energy of OOH to Pt sites of XPt_2 and X_2Pt is slightly reduced with respect to that in Pt_3.

The adsorbed OOH has a net negative charge resulting in a repulsive interaction with the adsorbent site, also negatively charged. We find that the magnitude of such repulsive force, represented by the square of the net OOH charge (Fig. 5), is directly proportional to the separation between the O atoms, except for structure B (see Table 2 or Fig. 3) which corresponds to the case when no foreign metal is part of the metallic cluster.

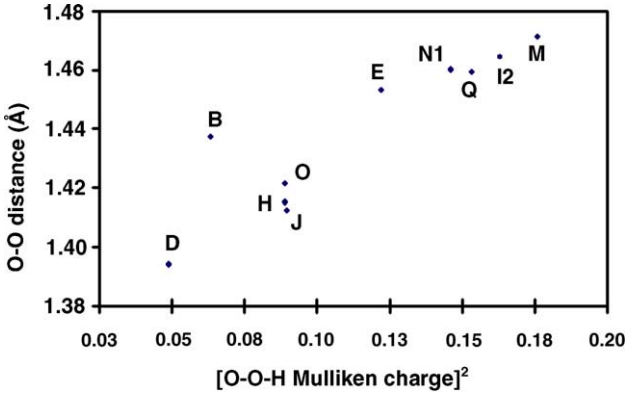

Fig. 5. Relation between the O–O distance and the square of the Mulliken charges for OOH adsorbed on Pt_3 and on the bimetallic clusters. The structures, which are represented by the letters defined in Table 2 and Fig. 3, correspond to the cases where OOH converged to an atop-site.

4. Conclusions

It is shown that Cr, Co, and Ni are better adsorption centers for OOH than Pt, but such strong adsorption might not favor the dissociation of OOH into adsorbed O and OH as expected in the catalyzed oxygen reduction. However, the presence of a different metallic atom in the vicinity of a Pt atom increases its electron density, enhancing the Pt ability to adsorb and transfer electrons to oxygenated species. Thus, the presence of Ni, Cr, and Co sites in the subsurface, rather than on the exposed surface, may contribute favorably to making Pt a better center for electron transfer and adsorption of oxygenated species. On the other hand, ensembles containing two Cr atoms are found able to dissociate OOH without barrier.

Acknowledgments

Financial support from the Department of Energy/Basic Energy Sciences, (DE-FG02-04ER15619) and from DURIP/ARO (Grant No. W911N F-04-1-0098) is gratefully acknowledged. The use of computational facilities at the National Energy Research Scientific Computing Center, NERSC, is appreciated.

References

[1] R.W. Reeve, P.A. Christensen, A.J. Dickinson, A. Hamnett, K. Scott, Electrochim. Acta 45 (2000) 4237.
[2] T. Tada, H. Igarahi, M. Watanabe, J. Electroanal. Chem. 460 (1999) 258.

[3] J.F. Drillet, A. Ee, J. Friedeman, R. Kotz, B. Schnyder, V.M. Schmidt, Electrochim. Acta 47 (2002) 1983.
[4] P.B. Balbuena, D. Altomare, L.A. Agapito, J.M. Seminario, J. Phys. Chem. B 107 (2003) 13671.
[5] S. Mukerjee, S. Srinivasan, J. Electroanal. Chem. 357 (1993) 201.
[6] S. Mukerjee, S. Srinivasan, M.P. Soriaga, J. McBreen, J. Phys. Chem. A 99 (1995) 4577.
[7] V. Stamenkovic, T.J. Schmidt, P.N. Ross, N.M. Markovic, J. Phys. Chem. B 106 (2002) 11970.
[8] A. Damjanovic, V. Brusic, Electrochim. Acta 12 (1967) 615.
[9] A. Damjanovic, D.B. Sepa, M.V. Vojnovic, Electrochim. Acta 24 (1979) 887.
[10] E.B. Yeager, Electrochim. Acta 29 (1984) 1527.
[11] E. Yeager, M. Razaq, D. Gervasio, A. Razaq, D. Tryk, J. Serb. Chem. Soc. 57 (1992) 819.
[12] P.D. Nolan, B.R. Lutz, P.L. Tanaka, J.E. Davis, C.B. Mullins, J. Chem. Phys. 111 (1999) 3693.
[13] A.C. Luntz, M.D. Williams, D.S. Bethune, J. Chem. Phys. 89 (1988) 4381.
[14] T. Li, P.B. Balbuena, Chem. Phys. Lett. 367 (2003) 439.
[15] Y. Wang, P.B. Balbuena, J. Phys. Chem. B 108 (2004) 4376.
[16] Y. Wang, P.B. Balbuena, J. Phys. Chem. B (submitted).
[17] R.A. Sidik, A.B. Anderson, J. Electroanal. Chem. 528 (2002) 69.
[18] N.M. Markovic, P.N. Ross, in: A. Wieckowski (Ed.), Interfacial Electrochemistry, Theory, Experiment and Applications, Marcel Dekker, New York, 1999, p. 821.
[19] R. Adzic, in: J. Lipkowski, P.N. Ross (Eds.), Electrocatalysis, Wiley-VCH, New York, 1998, p. 197.
[20] M.J. Frisch et al., GAUSSIAN-2003, Revision B.5., Gaussian, Inc., Pittsburgh, PA, 2003.
[21] P. Hohenberg, W. Kohn, Phys. Rev. B 136 (1964) 864.
[22] W. Kohn, L.J. Sham, Phys. Rev. A 140 (1965) 1133.
[23] A.D. Becke, J. Chem. Phys. 98 (1993) 5648.
[24] J.P. Perdew, Y. Wang, Phys. Rev. B 45 (1992) 13244.
[25] J.P. Perdew, J.A. Chevary, S.H. Vosko, K.A. Jackson, M.R. Pederson, D.J. Singh, C. Fiolhais, Phys. Rev. B 46 (1992) 6671.
[26] J.M. Seminario, J.M. Tour, Mol. Electron.: Sci. Technol. 852 (1998) 68.
[27] J.M. Seminario, A.G. Zacarias, J.M. Tour, J. Am. Chem. Soc. 122 (2000) 3015.
[28] W.R. Wadt, P.J. Hay, J. Chem. Phys. 82 (1985) 284.
[29] P.J. Hay, W.R. Wadt, J. Chem. Phys. 82 (1985) 299.
[30] P.J. Hay, W.R. Wadt, J. Chem. Phys. 82 (1985) 270.
[31] M.J. Frisch, J.A. Pople, J.S. Binkley, J. Chem. Phys. 80 (1984) 3265.
[32] A.K. Wilson, T. vanMourik, T.H. Dunning, J. Mol. Struct. – Theochem. 388 (1996) 339.
[33] R.A. Kendall, T.H. Dunning, R.J. Harrison, J. Chem. Phys. 96 (1992) 6796.
[34] D.E. Woon, T.H. Dunning, J. Chem. Phys. 98 (1993) 1358.
[35] O. Farkas, H.B. Schlegel, Phys. Chem. Chem. Phys. 4 (2002) 11.